

Identification of overlapping resonances in dissociative electron attachment to chlorine molecules

Pamir Nag and Dhananjay Nandi*

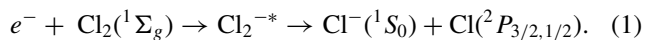
Indian Institute of Science Education and Research Kolkata, Mohanpur 741246, India

(Received 5 November 2015; published 5 January 2016)

A combined highly differential momentum imaging experiment and *ab initio* potential-energy curve calculation using density-functional theory (DFT) have been performed to understand the broad resonant peak around 5.7 eV due to dissociative electron attachment (DEA) to the chlorine molecule. Both the kinetic energy and angular distribution over the entire 2π angle of the fragment negative ions have been measured. Two heavily overlapping resonances are identified for the observed broad resonant peak that could settle the long-standing debate. The symmetry of the involved two temporary negative ion (TNI) states are determined from the angular distribution data. Experimental observations are strongly supported with the computed potential-energy curve using DFT.

DOI: [10.1103/PhysRevA.93.012701](https://doi.org/10.1103/PhysRevA.93.012701)**I. INTRODUCTION**

Chlorine (Cl_2) is a simple but important diatomic molecule, widely used in semiconductor and thin-film manufacturing [1]. It is having a high impact in environmental science and is responsible for ozone layer depletion [2]. Electron collision with Cl_2 plays a central role in plasma processes and excimer lasers [3]. Although plasma processes are largely electron driven, that electron induced reaction dynamics of Cl_2 is not yet completely understood might be due to primarily its high reactive nature and/or the lack of suitable experimental tools. Sophisticated experimental setups have been developed in recent times that can probe to understand kinematically complete dynamics in a reaction process. For low-energy electron collision with molecules, dissociative electron attachment (DEA) is a nice tool to study resonances and underlying dynamics [4,5]. DEA is in general a two-step process: In the first step, the electron is resonantly captured by the molecule forming a temporary negative ion (TNI) state that is in general unstable and repulsive in nature. In the second step, the TNI dissociates into final products of fragment negative ion and neutral(s). DEA to chlorine results in a Cl^- ion and a neutral Cl fragment, through the following process:



Previous experimental studies [6–9] using a high-resolution electron beam showed several structures in the DEA cross section. Three resonances, at near 0, 2.5 eV, and a broad peak around 5.7 eV, were observed experimentally. The first two resonances were well studied both theoretically [10–12] and experimentally [13–15] using a variety of techniques and conclusively assigned a $^2\Sigma_u^+$ and a $^2\Pi_g$ TNI state for each resonance, respectively.

At the current level of understanding, there could be three ways to identify different resonances experimentally by measuring (i) a cross section with a high-resolution electron beam source, (ii) kinetic energy, and (iii) angular distribution of fragment negative ions produced from DEA around the particular resonance. A long-standing debate regarding the involvement of TNI states for the third resonant peak of Cl^-/Cl_2 still exists in the literature. Kurepa and Belić [6]

reported the presence of a fourth resonance due to the $^2\Sigma_g^+$ state, hardly noticeable on the tail of the third resonance (due to the $^2\Pi_u$ TNI state). Recently, even with a very high-resolution (~ 80 meV) electron beam, Feketeova *et al.* [9] were not able to observe the presence of two separate resonances in their ion yield curve, and instead observed a broad peak around 5.5 eV. This suggests that the fourth resonance, if present at all, is highly overlapped with the third one. Theoretically [16] four Cl_2^- states are present around the DEA energy range; in order of increasing energy these are $^2\Sigma_u^+$, $^2\Pi_g$, $^2\Pi_u$, and $^2\Sigma_g$. Based on this ordering Feketeova *et al.* [9] assigned a $^2\Pi_u$ state for this resonance. Although, the $^2\Sigma_g^+$ state is also present, the authors excluded this state since it lies above the $^2\Pi_u$ state. Moreover, the computed $^2\Pi_u$ and $^2\Sigma_g^+$ states are out of the Franck-Condon overlap region in the measured energy range. The electron stimulated desorption (ESD) of Cl^- ions from condensed phase Cl_2 showed some close resemblance with dissociative electron attachment (DEA) to Cl_2 and the same $^2\Pi_u$ TNI states were assigned for the near 5.5-eV resonance [17]. All the above assignments were done based on energetics only. To understand the total number of TNI states and their symmetries involved in the process it is necessary to perform kinetic-energy and angular distribution measurements of fragment negative ions. There exists no kinetic-energy distribution and only one angular distribution measurement [8] of Cl^- arising from DEA to Cl_2 over a limited angular range. Based on angular distribution studies Azria *et al.* [8] concluded that the observed structure in the Cl^- ion yield curve in the energy range 4–8 eV could be due to either (i) a change with energy of the mixing of two partial waves in the single resonant ($^2\Pi_u$) state or (ii) due to a small contribution of the $^2\Sigma_g^+$ state below the $^2\Pi_u$ resonant state. But the $^2\Sigma_g^+$ state is always above the $^2\Pi_u$ state in all theoretically computed potential-energy curves. The lack of convergence between theory and experiment and unresolved questions regarding the structure of the ion yield curve demand further experimental and theoretical study for this resonance.

In this article we propose and give a clear evidence of the presence of two overlapping resonances around the 5.7-eV peak using the velocity slice imaging (VSI) technique. Unlike many-particle fragmentation dynamics, the recent development of a conceptually simpler, albeit powerful, velocity map imaging technique [18] in combination with a slicing

*dhananjay@iiserkol.ac.in

idea [19] have been successfully employed in the low-energy electron-molecule collision studies [20]. The application of VSI provided a sophisticated tool for simultaneous measurement of both kinetic energy and angular distribution over the entire 2π angle with higher efficiency. Here, we particularly focus on the symmetry determination of the Cl_2^- resonant state(s) responsible for the broad resonance of Cl^- formation around 5.7 eV due to DEA to chlorine molecules. By measuring both the kinetic energy and angular distribution of the fragment negative ions using the VSI technique [20] in our earlier studies [21,22], we could identify two closely lying resonances. But, the presently studied resonance seems to be heavily overlapped. However, those overlapping resonances could be identified based on angular distribution analysis and comparing that with the signatures observed in the kinetic-energy distribution and the ion yield curve. Involvement of a $^2\Pi_u$ and a $^2\Sigma_g^+$ TNI state around this peak have been observed experimentally. The potential-energy curves of the neutral chlorine molecule and molecular negative ions have been computed using the *ab initio* method that strongly supports our observations. Furthermore, all four calculated TNI states exactly match the experimentally observed resonant energies [9] for the DEA to chlorine molecules.

II. INSTRUMENTATION

The present experiments were performed using a highly differential momentum imaging technique. The apparatus is the same as that employed to study DEA to CO [21] and CO_2 [23] and similar to the earlier report of Nandi *et al.* [20]. Some details of the current experimental setup can be found elsewhere [24]. In brief, the setup consists of a custom designed pulsed electron gun, a Faraday cup to measure the electron-beam current, a capillary tube to produce an effusive molecular beam, and a velocity map imaging (VMI) spectrometer to record the momentum distribution of the ions. The electron-beam energy resolution for the current experiment in the presence of highly reactive chlorine appears to be around 1.2 eV, poorer than our previous reports. The entire experimental setup is mounted inside an oil-free vacuum chamber having a base pressure below $\sim 10^{-9}$ mbar and the chamber was heated at 130 °C for several days before performing the experiment to remove any impurities that might be present inside the chamber. The magnetically well collimated pulsed electron beam of 10 kHz repetition rate and 200 ns duration with controllable energy is made to interact perpendicularly with the effusive molecular beam. The electron beam is collimated by a uniform magnetic field of about 40 G, produced from a pair of magnetic coils in Helmholtz configuration situated outside the vacuum chamber. The negative ions are produced in the interaction region due to an electron captured by the isolated molecules. The created ions are extracted from the interaction region of the VMI spectrometer using a negative pulsed extraction field of 4 μs width applied 100 ns after the electron-beam pulse passed away. The delayed extraction provides an appropriate time spread in the time of flight (TOF) of the ions for better time slicing and also prevents the electrons from reaching the detector. Using the VMI condition all the ions created with a given velocity are mapped to a point on a two-dimensional

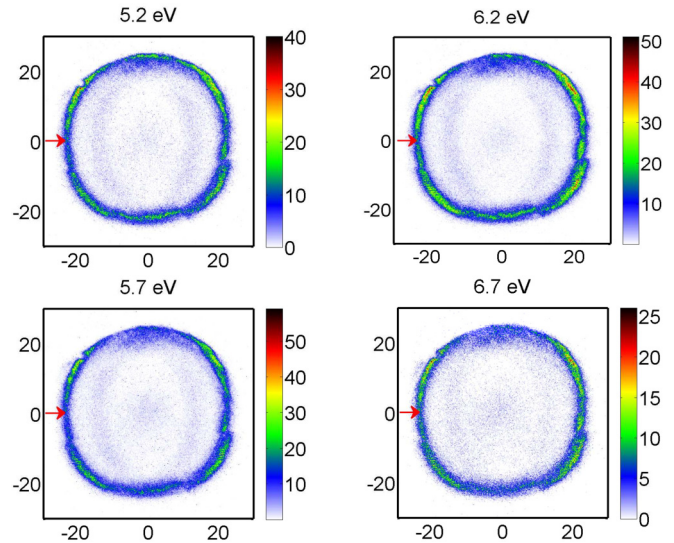


FIG. 1. Velocity slice images of Cl^- ions produced due to DEA to Cl_2 for different incident electron energies as stated. The electron-beam direction is from left to right and through the center of each image as indicated by arrows.

position sensitive detector (PSD) irrespective of their initial place of birth in the interaction zone. A combination of delay line hexanode [25] with three microchannel plates (MCPs) in Z-stack configuration are used as the position sensitive detector. The x and y positions of each detected ion are calculated from the three anode layers [25] placed behind the MCPs whereas information about the time of flight (TOF) of the corresponding detected ions are determined from the back MCP signal. The x and y position along with the TOF of each detected particle are acquired and stored in a list-mode format (LMF) using the CoboldPC software from RoentDek. The same software has been used to get the central slice through the negative ion “Newton sphere” containing the full angular and translational energy information. The time sliced image corresponds to the ions ejected in the plane parallel to the detector and containing the electron-beam axis. By selecting the appropriate time window during the off-line analysis of the stored LMF file one can get the central slice images as shown in Fig. 1.

The typical full width at half maximum (FWHM) of the TOF of the Cl^- ions produced from Cl_2 around the 5.7-eV resonance is about 1200 ns. A 50-ns thin time window has been appropriately chosen for each set of data to obtain the central part of the Newton sphere that contains complete information. The electron-beam energy calibration is performed using a 6.5-eV DEA peak of O^-/O_2 [26]. To determine the kinetic-energy distribution of the Cl^- ions from the sliced images, the spectrometer is calibrated with the kinetic-energy release of O^-/O_2 [27] and considering that the square of the radius of the image is proportional to the kinetic energy of the ions [28].

III. RESULTS AND DISCUSSION

The experiments have been performed with 99.9% pure commercially available chlorine gas. In this study, our main emphasis is on the broad resonance around 5.5 eV [9]. Previous

electron stimulated desorption (ESD) spectra [17] of Cl^- from multilayer Cl_2 also showed the presence of a structureless broad resonance around the same energy. Although from the study of DEA to Cl_2 in the gas phase with a high-resolution electron beam (~ 80 meV) no structure was observed [9] in the ion yield curve but in electron stimulated desorption (ESD) spectra of Cl^- ions from submonolayer Cl_2 on Xe gas films two structures at 5.0 and 6.2 eV for a particular 45° angle were observed [17]. Electron stimulated desorption (ESD) from a submonolayer can be described as a DEA on a molecular site and the TNI state(s) formed in the process should be similar with the gas phase DEA process. However, there might be a possible shift in the energy scale due to the presence of the environment. The observed structures in the ESD study with submonolayer Cl_2 could be due to the presence of more than one strongly overlapped resonances as in the case of DEA to gas phase Cl_2 . To conclusively know about the symmetries of the TNI states involved in the DEA process the angular distribution measurement of the fragment negative ions is necessary. In the following we determine both the kinetic energy and the angular distribution over the entire 2π angle with higher accuracy and efficiency using the VSI technique.

The velocity sliced images taken at different indicated incident electron energies around the studied resonance are shown in Fig. 1. The arrows indicate the direction of the incident electron beam. Unlike our previous studies [21,22] we do not observe any noticeable change in the images as the incident electron energy changes. However, close inspection of the sliced images show the presence of some faint ring pattern with smaller diameter. We believe these are coming from some chloride impurities created in the chamber and the gas line due to the reactions with highly reactive pure chlorine gas. The Cl^- ions created due to the electron collision with pure Cl_2 also shows two closely lying ring patterns; these could be due to the presence of two isotopes, e.g., ^{35}Cl and ^{37}Cl . To check that these are not an experimental artifact we have performed experiments with O^-/CO and O^-/O_2 without changing the experimental conditions before and after taking the images for Cl^-/Cl_2 and found the momentum distribution as expected [21,29]. These sliced images contain both the kinetic-energy and angular distribution information.

The available energy in the process is distributed among the neutral Cl atoms and the Cl^- ions. The kinetic energy of the Cl^- ions can be obtained from the energy and momentum conservation as

$$E_R = \frac{1}{2}[V_e - (D - A + E^*)], \quad (2)$$

where V_e is the energy available to the center-of-mass system, basically the incident electron energy. $D = 2.51$ eV is the dissociation energy of the neutral Cl_2 molecule, $A = 3.61$ eV, is the electron affinity of the Cl atom, and E^* is the excitation energy of the neutral Cl atom with value 0 and 0.109 eV for $^2P_{3/2}$ and $^2P_{1/2}$ states respectively [30]. The observed kinetic-energy distributions from each image are shown in Fig. 2. Considering the 1.2-eV energy spread in the primary electron-beam the dominant peak around 2.8 eV fairly matches the value calculated from thermochemical parameters within the experimental uncertainty. In the kinetic-energy distribution curve of Cl^- ions for 4.7 eV incident electron energy a structure

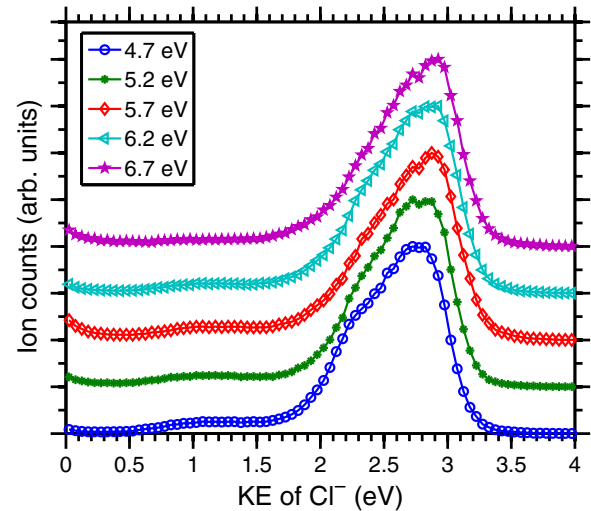


FIG. 2. Kinetic-energy distribution of Cl^- ions arising from DEA to Cl_2 taken at indicated electron energies.

within the dominant peak can be observed, for 5.2 eV the structure becomes less prominent and is gradually converted into a broad structureless peak as the incident electron energy increases, although from the measured kinetic-energy distribution it is hard to conclude about the states involved in the DEA process, as for a given electron energy and with only one dissociation limit a single kinetic-energy peak is expected. But the presence of the structure at the lower energy side might be a signature of the involvement of two resonant states discussed latter.

The angular distributions of the Cl^- ions created due to different incident electron energies around the 5.7-eV resonance are shown in Fig. 3. As already discussed, both ^{35}Cl and ^{37}Cl isotopes might be present in the sample gas and during angular distribution measurement all the Cl^- ions created with kinetic energy between 1.8 and 3.5 eV are considered, we expect that the effect of isotopes will not appear in the measured angular distribution. The angular distributions peak at around the 40° , 90° , and 140° directions. A nonzero intensity is observed in the forward (0°) and backward (180°) directions and that increases with an increase in incident electron energy. Being a homonuclear diatomic molecule, no forward-backward asymmetry is expected and also is not observed. From the angular distribution of the Cl^- ions, the symmetry of the TNI states of Cl_2^- has been determined. The angular distribution of the fragment ions created by DEA to a diatomic molecule can be expressed using the general expression given by O'Malley and Taylor [31],

$$I(k, \theta, \phi) \sim \left| \sum_{L=|\mu|}^{\infty} a_{L,|\mu|}(k) Y_{L,\mu}(\theta, \phi) \right|^2, \quad (3)$$

due to the involvement of each resonant state. Where k is the incident electron momentum, $a_{L,|\mu|}$ are energy-dependent expansion coefficients for each partial wave expressed by the spherical harmonics $Y_{L,\mu}$. If the projection of the electronic axial orbital momentum along the molecular axis for the initial and final states are Λ_i and Λ_f respectively then

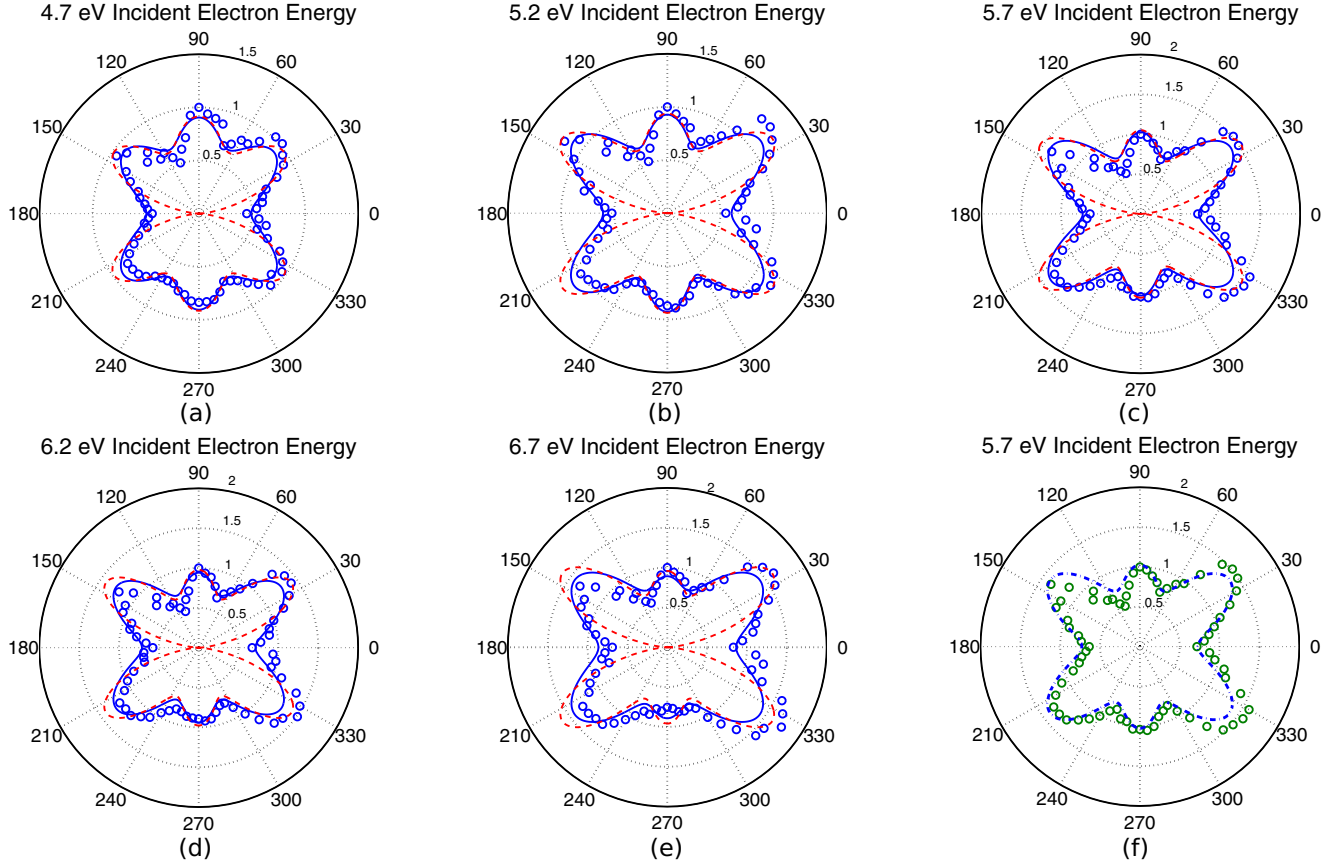


FIG. 3. The experimentally observed normalized angular distributions of Cl^- ions created due to DEA to Cl_2 having kinetic-energy range 1.8–3.5 eV are displayed using the scattered plot. (a)–(e) The fitted curve for $\Sigma_g \rightarrow \Pi_u$ and $\Sigma_g \rightarrow \Sigma_g + \Pi_u$ transition are shown using the red dashed and blue solid curves, respectively. (f) The angular distribution for 5.7 eV fitted with $\Sigma_g \rightarrow \Sigma_g$ transition is shown using the blue broken line for a comparison with (c).

$\mu = |\Lambda_f - \Lambda_i|$. The angular momentum quantum numbers (L) are restricted to even or odd values depending on whether the initial and final states are having the same or opposite parity and allowed values are $L \geq |\mu|$. Here, due to the involvement of one or more state(s) the angular distributions have been fitted using the modified expression by Tronc *et al.* [32],

$$I(\theta) \sim \sum_{|\mu|} \left| \sum_{j=|\mu|} a_j Y_{j,\mu} e^{i\delta_j} \right|^2. \quad (4)$$

The summation over μ takes care of the involvement of more than one final state. The δ_j s are the phase differences between the partial waves with respect to the lowest one involved in the process. During the analysis of the angular distribution, Dunn's selection rules [33] for homonuclear diatomic molecule have

been taken into account. The different fitting parameters used for $\Sigma_g \rightarrow \Pi_u$ and $\Sigma_g \rightarrow \Sigma_g + \Pi_u$ transitions are listed in Tables I and II, respectively. The best fitted curve for $\Sigma_g \rightarrow \Pi_u$ and $\Sigma_g \rightarrow \Sigma_g + \Pi_u$ transitions are shown using a red broken line and blue solid curve respectively in Figs. 3(a)–3(e) for five different incident electron energies, whereas the best fitted curve with only a $\Sigma_g \rightarrow \Sigma_g$ transition for 5.7 eV is shown as a blue broken line in Fig. 3(f) for comparison with Fig. 3(c).

We have computed the potential-energy curve for the neutral Cl_2 molecule in ground and different negative molecular ion states by density-functional theory (DFT) calculation using the MOLPRO package [34,35]. The B3LYP functional with 6-311++G** basis set is used in the calculation. Being a homonuclear diatomic molecule both Cl_2 and Cl_2^- belong to $D_{\infty h}$ point-group symmetry but MOLPRO uses only Abelian

TABLE I. Fitting parameters for the angular distribution of the Cl^- ions. The angular distributions are fitted with Σ_g to Π_u transition.

	4.7 eV	5.2 eV	5.7 eV	6.2 eV	6.7 eV
Weighting ratio of different partial waves					
$b_1 : b_3$	1: 0.669	1: 0.748	1: 0.795	1: 0.803	1: 0.805
Phase difference					
δ_{p-f} (rad)	1.374	1.326	1.289	1.294	1.221

TABLE II. Fitting parameters for the angular distribution of the Cl^- ions. The angular distributions are fitted with Σ_g to Σ_g and Π_u transition.

	4.7 eV	5.2 eV	5.7 eV	6.2 eV	6.7 eV
Weighting ratio of different partial waves					
$a_0: a_2: a_4:$	1: 1.224: 2.397:	1: 0.408: 0.876:	1: 0.556: 0.636:	1: 0.367: 0.353	1: 0.129: 0.316
$b_1: b_3$	8.684: 5.652	2.828: 1.892	1.973: 1.624	0.791: 0.937	1.204: 0.864
Phase difference (Σ_g)					
$\delta_{s-d}, \delta_{s-g}$ (rad)	3.977, 3.292	0.199, 1.769	1.244, 2.432	2.685, 1.582	0.397, 1.556
Phase difference (Π_u)					
δ_{p-f} (rad)	4.870	1.371	1.452	0.937	1.174

point-group symmetry [36] so D_{2h} point-group symmetry for the present case is used. The orbitals of the chlorine molecule and molecular negative ions with symmetries belonging to the $D_{\infty h}$ point group are represented in terms of the symmetries of the D_{2h} point group [37]. The ground state of neutral Cl_2 , i.e., $^1\Sigma_g^+$ ($\dots, 5\sigma_g^2, 2\pi_{ux}^2, 2\pi_{uy}^2, 2\pi_{gx}^2, 2\pi_{gy}^2$), the ground state of Cl_2^- molecular ion $^2\Sigma_u$ with configuration $\dots, 2\pi_{gx}^2, 2\pi_{gy}^2, 5\sigma_u^1$, and three more excited states of Cl_2^- having a single hole in close-shell configuration $^2\Pi_g$ ($\dots, 2\pi_{gx}^2, 2\pi_{gy}^1, 5\sigma_u^2$), $^2\Pi_u$ ($\dots, 5\sigma_g^2, 2\pi_{ux}^1, 2\pi_{uy}^2, 2\pi_{gx}^2, 2\pi_{gy}^2, 5\sigma_u^2$), and $^2\Sigma_g$ ($\dots, 5\sigma_g^1, 2\pi_{ux}^2, 2\pi_{uy}^2, 2\pi_{gx}^2, 2\pi_{gy}^2, 5\sigma_u^2$), are computed over a wide energy range and shown in Fig. 4. From the potential-energy curve it is evident that in the Franck-Condon overlap region around a 5.7-eV energy difference in both $^2\Pi_u$ and $^2\Sigma_g$ states is present and may be involved in the DEA process. The Franck-Condon overlap region with the $^2\Pi_u$ state starts at around 4 eV and continues until nearly 6 eV whereas the overlap with the $^2\Sigma_g$ state starts at around 5 eV and continues until nearly 7 eV. The overlapped region is shown using vertical lines in Fig. 4.

From the computed potential-energy curve and the experimentally observed kinetic energy and angular distribution one

can conclusively assign that two overlapping resonances are responsible for the broad resonant peak in the ion yield curve. From the computed potential+energy curve (Fig. 4), it is also obvious that the Franck-Condon region starts at 4 eV and continues nearly up to 7 eV and could result in the resonance over the broad energy range.

As already discussed in the kinetic+energy distribution for 4.7 eV, a structure has been observed that reduced at 5.2 eV and converted into a structureless broad peak for higher incident electron energies. Although for a single incident electron energy and only one bond dissociation limit only a single kinetic+energy peak is expected, but it might be possible that for lower incident electron energy the overlap is not too strong. As discussed earlier, the energy spread of the electron beam is about 1.2 eV. Due to the resonant nature of the DEA process, for a given incident electron energy, electrons with lower and higher energy tails within the broad energy distribution might be selectively attached with the molecule and could form a $^2\Pi_u$ or $^2\Sigma_g^+$ TNI state. This could explain the observed double structures in the kinetic-energy distribution curve for low incident electron energy. But as the incident electron energy increases, the overlap in the transition probability between the two states increases and as a result the selectiveness may disappear and the two structures in the kinetic-energy distribution appears as a single broad peak as observed. It can also be observed from the computed potential-energy curve (Fig. 4) that the strong overlap in the transition probability between Π_u and Σ_g states starts around 5.2 eV only.

Previously, Azria *et al.* [8] fitted their observed angular distribution data over a limited angular range between 20° and 120° with either a $\Sigma_g \rightarrow \Pi_u$ or $\Sigma_g \rightarrow \Sigma_g$ transition model. They could successfully describe the angular distribution data with the above model, however, the issue for a broad resonant peak in the ion yield was not resolved. They were successful to fit their data with either of two models due to the lack of data in the forward and backward directions. We also observed that within the same angular range both models can explain our observed angular distribution data, but the nonzero intensity in the forward and backward directions clearly indicate that only the Π_u state cannot explain [38] the experimentally observed angular distribution. According to Dunn's selection rule [33] for the homonuclear diatomic molecule a $\Sigma_g \rightarrow \Pi_u$ transition gives zero intensity in forward and backward directions but a nonzero intensity from a $\Sigma_g \rightarrow \Sigma_g$ transition. The next accessible TNI state of Cl_2^- just

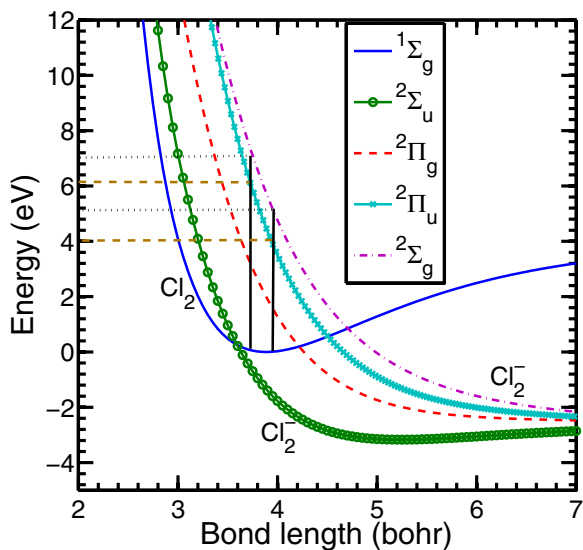


FIG. 4. Potential-energy curves of neutral ground-state chlorine and a few of its anionic states relevant for the DEA process. The potential-energy curves are obtained by DFT calculation using B3LYP functional with 6-311++G** basis set.

above the ${}^2\Pi_u$ state is a ${}^2\Sigma_g^+$ and may involve in the resonance. The intensity along the forward and backward directions increases with incident electron energy that clearly indicates the contribution of the ${}^2\Sigma_g^+$ TNI state increases as expected from the computed potential-energy curves also. Based on the fitted angular distribution curve one can argue that in principle only a $\Sigma_g \rightarrow \Sigma_g$ transition can describe the observed angular distribution, as shown in Fig. 3(f). But the observed broad resonance peak in the ion yield curve, the structures in kinetic energy distribution, and the increasing intensity along 0° and 180° in angular distribution cannot be explained with a single transition model. Electron stimulated desorption (ESD) study of Cl^- ions from condensed Cl_2 which strongly resembles the DEA to Cl_2 in gas phase [17] also shows some signature of the presence of two resonances. ESD of Cl^- the from submonolayer of Cl_2 on Xe gas film shows two structures at 5.0 and 6.2 eV only at a particular angle 45° and one should remember that the DEA cross section of Cl^-/Cl_2 is angle dependent and gives a peak around 40° for a $\Sigma_g \rightarrow \Pi_u + \Sigma_g$ transition. So, the presence of two overlapping resonances could be the reason for observing two peaks only around 45° by Tegeder *et al.* [17] in condensed Cl_2 . Although our angular distribution results are well fitted with either a single Σ_g TNI

state or Σ_g plus Π_u TNI states, we strongly accept the latter one in order to explain all the experimentally observed features in the DEA to Cl_2 .

IV. CONCLUSION

We have demonstrated a complete understanding of the DEA process to the Cl_2 molecule particularly for the broad resonant peak around 5.7 eV. Combining experimental observations with the theoretical potential-energy curve calculation we showed strong evidence for the presence of two heavily overlapped resonances. Our conclusion can successfully describe the ion yield curve observed [9] due to electron collision to both the gas phase and condensed phase [17] chlorine molecule. This study can resolve the long-standing debate that exists in the literatures.

ACKNOWLEDGMENTS

D.N. gratefully acknowledges the partial financial support from “Indian National Science Academy” for the development of the VSI spectrometer under INSA Young Scientist project SP/YSP/80/2013/734.

-
- [1] M. Kimura and Y. Itikawa, *Electron Collisions with Molecules in Gases: Applications to Plasma Diagnostics and Modeling* (Academic, New York, 2000), Vol. 44.
- [2] R. P. Wayne, *Chemistry of Atmospheres* (Oxford University Press, New York, 1993).
- [3] E. W. McDaniel and W. L. Nighan, *Gas Lasers: Applied Atomic Collision Physics* (Academic, New York, 1982), Vol. 3.
- [4] E. Illenberger and J. Momigny, *Gaseous Molecular Ions: An Introduction to Elementary Processes Induced by Ionization*, Topics in Physical Chemistry (Steinkopff-Verlag, Heidelberg, 1992).
- [5] T. Märk and G. Dunn, *Electron Impact Ionization* (Springer, Vienna, 2013).
- [6] M. V. Kurepa and D. S. Belić, *J. Phys. B* **11**, 3719 (1978).
- [7] W. Tam and S. F. Wong, *J. Chem. Phys.* **68**, 5626 (1978).
- [8] R. Azria, R. Abouaf, and D. Teillet-Billy, *J. Phys. B* **15**, L569 (1982).
- [9] L. Feketeova, D. Skalny, G. Hanel, B. Gstir, M. Francis, and T. Märk, *Int. J. Mass Spectrom.* **223-224**, 661 (2003).
- [10] T. Leininger and F. X. Gadéa, *J. Phys. B* **33**, 735 (2000).
- [11] I. I. Fabrikant, T. Leininger, and F. X. Gadéa, *J. Phys. B* **33**, 4575 (2000).
- [12] P. W. Tasker, G. G. Balint-Kurti, and R. N. Dixon, *Mol. Phys.* **32**, 1651 (1976).
- [13] S. Barsotti, M.-W. Ruf, and H. Hotop, *Phys. Rev. Lett.* **89**, 083201 (2002).
- [14] R. J. Gulley, T. A. Field, W. A. Steer, N. J. Mason, S. L. Lunt, J.-P. Ziesel, and D. Field, *J. Phys. B* **31**, 2971 (1998).
- [15] L. G. Christophorou and J. K. Olthoff, *J. Phys. Chem. Ref. Data* **28**, 131 (1999).
- [16] T. L. Gilbert and A. C. Wahl, *J. Chem. Phys.* **55**, 5247 (1971).
- [17] P. Tegeder, R. Balog, N. J. Mason, and E. Illenberger, *Phys. Chem. Chem. Phys.* **7**, 685 (2005).
- [18] A. T. J. B. Eppink and D. H. Parker, *Rev. Sci. Instrum.* **68**, 3477 (1997).
- [19] M. Ashfold, N. Nahler, A. Orr-Ewing, O. Vieuxmaire, R. Toomes, T. Kitsopoulos, I. Anton-Garcia, D. Chestakov, S.-M. Wu, and D. Parker, *Phys. Chem. Chem. Phys.* **8**, 26 (2006).
- [20] D. Nandi, V. S. Prabhudesai, E. Krishnakumar, and A. Chatterjee, *Rev. Sci. Instrum.* **76**, 053107 (2005).
- [21] P. Nag and D. Nandi, *Phys. Chem. Chem. Phys.* **17**, 7130 (2015).
- [22] D. Nandi, V. S. Prabhudesai, B. M. Nestmann, and E. Krishnakumar, *Phys. Chem. Chem. Phys.* **13**, 1542 (2011).
- [23] P. Nag and D. Nandi, *Phys. Rev. A* **91**, 052705 (2015).
- [24] P. Nag and D. Nandi, *Meas. Sci. Technol.* **26**, 095007 (2015).
- [25] O. Jagutzki, A. Cerezo, A. Czasch, R. Dörner, M. Hattas, M. Huang, V. Mergel, U. Spillmann, K. Ullmann-Pfleger, T. Weber, H. Schmidt-Böcking, and G. Smith, *IEEE Trans. Nucl. Sci.* **49**, 2477 (2002).
- [26] D. Rapp and D. D. Briglia, *J. Chem. Phys.* **43**, 1480 (1965).
- [27] D. Nandi and E. Krishnakumar, *Int. J. Mass Spectrom.* **289**, 39 (2010).
- [28] B. Whitaker, *Imaging in Molecular Dynamics: Technology and Applications* (Cambridge University Press, Cambridge, UK, 2003).
- [29] D. Nandi, V. Prabhudesai, and E. Krishnakumar, *Radiat. Phys. Chem.* **75**, 2151 (2006).
- [30] NIST Chemistry WebBook.
- [31] T. F. O'Malley and H. S. Taylor, *Phys. Rev.* **176**, 207 (1968).

- [32] M. Tronc, C. Schermann, R. I. Hall, and F. Fiquet-Fayard, *J. Phys. B* **10**, 305 (1977).
- [33] G. H. Dunn, *Phys. Rev. Lett.* **8**, 62 (1962).
- [34] H.-J. Werner, P. J. Knowles, G. Knizia, F. R. Manby, and M. Schütz, *Comput. Mol. Sci.* **2**, 242 (2012).
- [35] H.-J. Werner, P. J. Knowles, G. Knizia, F. R. Manby, M. Schütz *et al.*, Molpro, version 2012.1, a package of ab initio programs, 2012.
- [36] H. J. Werner and P. J. Knowles, Molpro, users manual version 2012.1, <http://www.molpro.net/info/2012.1/doc/manual.pdf>, 2012.
- [37] H. J. Werner and P. J. Knowles, Molpro, getting started with molpro, version 2012.1, <http://www.molpro.net/info/2012.1/doc/quickstart.pdf>, 2012.
- [38] V. S. Prabhudesai, D. Nandi, and E. Krishnakumar, *J. Phys. B* **39**, L277 (2006).